

# Is directed percolation class for synchronization transition robust with multi-site interactions?

Manoj C. Warambhe<sup>1,2</sup> and Prashant M. Gade<sup>2</sup>

<sup>1</sup> Department of CSE, GH Rasoni Skill Tech University, Nagpur, India

<sup>2</sup> Department of Physics, RTM Nagpur University, Nagpur, India

**Abstract.** Coupled map lattice with pairwise local interactions is a well-studied system. However, in several situations, such as neuronal or social networks, multi-site interactions are possible. In this work, we study the coupled Gauss map in one dimension with 2-site, 3-site, 4-site and 5-site interaction. This coupling cannot be decomposed in pairwise interactions. We coarse-grain the variable values by labeling the sites above  $x^*$  as up spin (+1) and the rest as down spin (-1) where  $x^*$  is the fixed point. We define flip rate  $F(t)$  as the fraction of sites  $i$  such that  $s_i(t-1) \neq s_i(t)$  and persistence  $P(t)$  as the fraction of sites  $i$  such that  $s_i(t') = s_i(0)$  for all  $t' \leq t$ . The dynamic phase transitions to a synchronized state is studied above quantifiers. For 3 and 5 sites interaction, we find that at the critical point,  $F(t) \sim t^{-\delta}$  with  $\delta = 0.159$  and  $P(t) \sim t^{-\theta}$  with  $\theta = 1.5$ . They match the directed percolation (DP) class. Finite-size and off-critical scaling is consistent with DP class. For 2 and 4 site interactions, the exponent  $\delta$  and behavior of  $P(t)$  at critical point changes. Furthermore, we observe logarithmic oscillations over and above power-law decay at the critical point for 4-site coupling. Thus multi-site interactions can lead to new universality class(es).

## 1 Introduction

A complex network has many interacting components that show the various range of dynamical behaviour[1,2]. Such a system is applicable in many real-world systems, including the spreading of diseases in the populations [3], complex biological pathways [4], social networks [5], neuronal networks [1,6] etc. Dynamical systems on such networks could be coupled differential equations, coupled maps (CML), or cellular automata with a decreasing degree of complexity. Most of these models involve pairwise interactions between different elements. However, there are many systems where multi-site interaction is possible. This higher-order interaction is usually more complex and studied in many fields of science such as physics [7], mathematics [8], and computer science [9]. For instance, higher-order interactions are useful for modeling the functional brain connections[10]. In this work, we study coupled maps with higher-order interactions. Map-based models have less computational cost and can reveal qualitative features. Such interactions can change the nature of dynamic phase transitions. Higher-order Kuramoto model can lead to explosive synchronization [11]. This is a discontinuous transition. The self-organized behavior of coupled-phase oscillators with many-body interaction is studied in [12]. This coupling reproduces the

rapid synchronization in many valid biological networks. It has hysteresis and bistability indicating first-order transition. Such multi-site couplings are often studied on simplicial geometries [13, 14, 15, 16]. There are several reports of first-order transition in systems with simplicial couplings [11, 17, 18, 19, 20]. CML of logistic maps or neuronal maps with simplicial coupling is studied in [21, 22]. The above systems, many of which have real-world applications, motivate us to study the higher-order interaction in a system of coupled chaotic maps.

In particular, we study the transition to synchronization. We study CML with multi-site interaction. In this model, we study coupled map lattice with 2-site, 3-site, 4-site, and 5-site interaction. We retain the one-dimensional nature of underlying topology so that it is possible to compare it with one-dimensional transitions. Firstly, we find that the nature of the transition can be continuous and not necessarily explosive. Standard finite-size scaling is observed. (In explosive synchronization, it is claimed that the finite-size scaling is atypical [23].) All exponents including relatively less universal persistence exponent match with expected values for one-dimensional DP for the 3-site and 5-site interaction. The situation changes for the 2-site or 4-site interaction.

The Gauss map is a 1D map based on the Gaussian exponential function [24]. Unlike logistic, tent, or circle maps, this is a map defined on the entire real line and not an interval. Such maps are relatively less studied. On changing the map parameter values, this map shows the diverse range of dynamical behaviour including reverse period doubling, period adding and chaos. In standard form, it can be defined as:

$$f(x) = \exp(-\nu x^2) + \beta, \quad x \in R \quad (1)$$

Where  $\nu$  and  $\beta$  are the control parameters of the given map. We plot the bifurcation diagram of the Gauss map for  $\nu = 7.5$  [see **Fig.1**]. We plot all sites as a function of map parameter  $\beta$ . The bifurcation plot displays distinct dynamical behavior including the reverse period-doubling, period-adding and chaos.

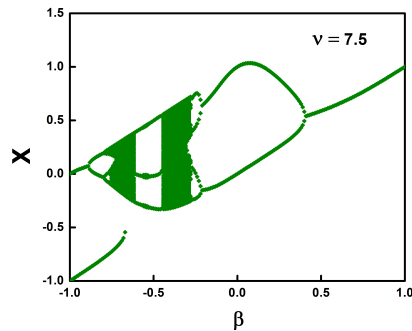


Fig. 1: Bifurcation diagram for Gauss map for  $\nu = 7.5$ . It shows the reverse period-doubling, period-adding as well as chaos.

We study the CML with multi-site interaction in the Gauss map with positive coupling. Our studies are the viewpoint of phase transition, and this phase transition is identified by the appropriate order parameter. We consider local persistence  $P(t)$  and flip rate  $F(t)$  as order parameters. Persistence is the probability that a nonequilibrium field value does not change the sign up to time  $t$  during stochastic evolution [25]. This is a non-Markovian quantity and experimental investigations are difficult for obvious

reasons. In several systems, persistence decays algebraically with time at the critical point as  $P(t) \sim t^{-\theta}$  where  $\theta$  is the decay exponent known as the persistence exponent. We need the knowledge of entire time evolution to find this quantity.

For CML, transition to a frozen or partially frozen state in a coarse-grained sense can be characterized by persistence and power-law behaviour may be obtained only at the critical coupling. However, the persistence exponent is not universal. As noted below, several 1D systems in the DP universality class have persistence exponent  $3/2$ , and several systems in directed Ising universality have persistence exponent unity [26]. The persistence exponent in the 1D DP model such as the Domany-Kinzel model [27], Ziff-Gulari-Barshed model [28], site percolation [29] and 1D circle map [30,31] is observed to be  $3/2$ . (We note that the synchronization transition between two coupled CML is found to be in bounded KPZ universality class for smooth maps[32]. But, we focus on a single CML in this work.) The transition to a random pattern is frozen in the coarse-grained state (not synchronized) can be in DP universality class in CML [33,34] and shows persistence exponent close to  $3/2$ . Although not universal, we can observe the same persistence exponent in a significant set of models belonging to the same universality class. Hence, it is important. In the above cases of coupled maps, flip rate  $F(t)$  is studied as a measure of lattice activity at a given time  $t$ . Recently, a new universality class pertaining to transition to a period  $n$  absorbing state has been observed in coupled map lattice and has been investigated using the flip rate as a quantifier[34]. (It is also modeled by the cellular automata model in [35].) We use the similar measure here. We denote sites with a variable value greater than a fixed point as spin (+1) and those with a value less than a fixed point as spin (-1). For the case of period-3 synchronization, flip rate is defined as the fraction of sites that change their spin state from state at time  $t - 3$ [34]. If the underlying coarse-grained periodicity is 2, it is the fraction of sites that changed its state at time  $t$  from the state at  $t - 2$ [21,33]. Thus, any departure from the expected underlying dynamics is the flip rate. In our case, the flip rate  $F(t)$  is the fraction of sites that change their spin state at  $t$  from the previous state at  $(t - 1)$ .

DP is the most widely observed universality class in the nonequilibrium system from the viewpoint of phase transition from the active state to the absorbing state. It is observed in several systems including transition to turbulence [36] or transition between two turbulent states of electroconvection in nematic liquid crystals [37]. Janssen–Grassberger conjecture [38,39] stated the conditions for DP transition as [39] “the universality class of DP contains all continuous transitions from a dead or absorbing state to an active one with a single scalar order parameter, provided the dead state is not degenerate and provided some technical points are fulfilled: short-range interactions both in space and time, the nonvanishing probability for any active state to die locally, translational invariance (absence of frozen randomness), and absence of multicritical points”. The question is whether all these conditions are necessary and what happens if we relax some or all of them. Relaxation in some of these conditions still leads to the directed percolation universality class[40]. Most of the models studied have pairwise interactions. We study interaction that cannot be decomposed as pairwise interaction and check the universality class of absorbing state transition in this system.

For CML with pairwise interaction, there are numerous instances of dynamic transitions in the DP universality class. For the coupled Gauss map, it has been observed that the transition to a frozen state in a coarse-grained sense is in DP universality class [33]. Chate and Manneville studied the coupled piecewise linear discontinuous map and showed that the transition led to DP class behavior [41]. It has been also shown that unidirectional coupling and asymmetric coupling are not relevant perturbations for the DP class [42]. In [40], the robustness of the DP class in the presence of recovery time, memory, external forcing, or quenched disorder was

checked. It was found that these perturbations do not alter the universality class of the transition. In this work, we find that the DP class is robust for coupled Gauss maps for 3-site and 5-site interaction. Thus some multi-site interactions are not a relevant perturbation to the DP universality class. However, for 2-site or 4-site interaction, we obtain new exponents, and the class changes.

## 2 The Model

We consider the following model. Consider a lattice of length  $N$ . We denote the local variable at site  $i$  as  $x_i(t)$ . The initial conditions are chosen as a uniform random number in the interval  $[0, 1]$ . We use the periodic boundary conditions. The evolution proceeds in a synchronous manner. The time evolution of  $x_i(t)$  at discrete time  $t$  for 2-sites, 3-site, 4-site and 5-site interaction are given by

$$x_i[t + 1] = (1 - \epsilon)f[x_i(t)] + \epsilon f[x_{i-1}(t)]f[x_{i+1}(t)] \quad (2)$$

$$x_i[t + 1] = (1 - \epsilon)f[x_i(t)] + \epsilon f[x_i(t)]f[x_{i-1}(t)]f[x_{i+1}(t)] \quad (3)$$

$$x_i[t + 1] = (1 - \epsilon)f[x_i(t)] + \epsilon f[x_{i-1}(t)]f[x_{i+1}(t)]f[x_{i-2}(t)]f[x_{i+2}(t)] \quad (4)$$

$$x_i[t + 1] = (1 - \epsilon)f[x_i(t)] + \epsilon f[x_i(t)]f[x_{i-1}(t)]f[x_{i+1}(t)]f[x_{i-2}(t)]f[x_{i+2}(t)] \quad (5)$$

where  $t$  is time index and  $i = 1, 2, 3, \dots, N$  is the site index. The difference from the usual CML is that this coupling cannot be decomposed in pairwise interactions. In the above equation,  $\epsilon$  is the coupling parameter, which is a measure of the strength of coupling between site  $i$  and its neighbours. At  $\epsilon = 0$  we recover the function  $f(x)$  and all sites evolve independently of each other. The function  $f(x)$  is the Gauss map which is defined in **Eq. 1**. Let,  $x^*$  be the non-zero fixed point of the Gauss map which is obtained using the bisection method. We associate spin is  $s_i(t)$  with site  $i$  at time  $t$ . If the variable value  $x_i(t) > x_i^*$ ,  $s_i(t) = 1$  and if  $x_i(t) < x_i^*$ ,  $s_i(t) = -1$ . We define two quantifiers local persistence  $P(t)$  and flip rate  $F(t)$  as follows:

**Persistence:** *The fraction of sites that did not alter their spin value even once throughout all time steps are referred to as persistent sites. The fraction of persistent sites denoted by  $P(t)$  is persistence at time  $t$ . Thus, the persistence  $P(t)$  at time  $t$  is fraction of sites  $i$  such that  $s_i(t') = s_i(0)$  for all  $t' \leq t$ .*

**Flip rate:** *Flip rate  $F(t)$  is the fraction of sites at time  $t$  that changed their spin state from the state at time  $(t - 1)$ . In other words, flip rate  $F(t)$  is the fraction of sites  $i$  such that  $s_i(t - 1) \neq s_i(t)$ .*

## 3 Results and Discussion

### 3.1 Coupled map lattice with 5-site interaction

First, we study our model for a 5-site interaction coupled Gauss map. The bifurcation diagram is the most simple method for displaying dynamic behavior while varying a control parameter. We plot the bifurcation diagram for the 5-site coupled Gauss map for map parameters  $\nu = 7.5$  and  $\beta = 0.8$  [see **Fig.2**]. We consider  $N = 500$  and wait for  $t = 10^5$ . The bifurcation diagram displays the all values of sites  $x_i(t)$  as a function of coupling parameter  $\epsilon$  at  $t = 10^5$ . The bifurcation plot shows a clear synchronization transition for a larger value of  $\epsilon$ , which we investigate in detail.

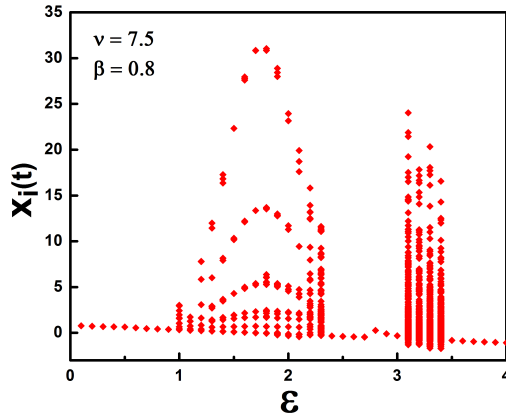


Fig. 2: Plot of bifurcation diagram for 5-site interaction coupled Gauss maps where  $x_i(t)$  is plotted as a function of  $\epsilon$ . We fix  $\nu = 7.5$  and  $\beta = 0.8$  and wait for  $t = 10^5$  time steps.

We also study the space-time diagram for visualizing the defects for the 5-site interaction coupled Gauss map. We plot it for discrete time  $t$  as a function of site index  $i$  (where  $i = 1, \dots, N$ ) for  $N = 100$  and  $\epsilon = 3.51475$ . The behavior of such defects is plotted in **Fig. 3 (a)** and in **Fig. 3 (b)**. (Defects are the sites for which  $|x_i(t) - x^*| > \eta$  where  $\eta = 0.1$ .) We observe the spatiotemporal intermittency (STI) in two different regions for both plots. There is no ‘*solitonlike*’ structure observed in this regime. A similar evolution is observed in [43] for coupled map lattice defined in a standard manner (see Figure 1 and Figure 2 of [43]).

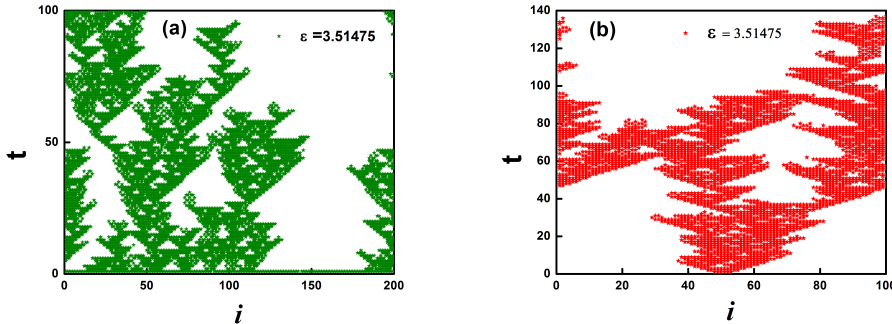


Fig. 3: **(a)** Space-time plot of defects for 5-site coupled Gauss map for  $N = 100$  and  $\epsilon = 3.51475$  for random initial conditions. **(b)** Space-time plot of defects for coupled Gauss map for  $N = 100$  and  $\epsilon = 3.51475$ . At  $t = 0$   $x(i, 0) = x^*$  for all  $i$  except three sites in the center.

Saturation of persistence usually implies that the activity has stopped fully or partially. Hence the synchronization is accompanied by saturation of persistence. Thus, the order parameter becoming zero is accompanied by saturation of persistence.

On the other hand, the active state will lead to persistence becoming zero if activity continues at all lattice sites. Thus, there is a critical value of coupling  $\epsilon_c$  such that for  $\epsilon > \epsilon_c$  the order parameter goes to zero and persistence saturates while for  $\epsilon < \epsilon_c$ , the order parameter saturates and persistence goes to zero. For continuous transition, we observe power-law decay of both persistence and order parameter at the critical point  $\epsilon_c$ . At such a critical point, the persistence and order parameter algebraically decays as:

$$P(t) \sim t^{-\theta} \quad (6)$$

$$O(t) \sim t^{-\delta} \quad (7)$$

The exponent  $\theta$  is known as the persistence exponent and  $\delta$  is the order parameter exponent. The exponents  $\theta$  are not universal and depend on the details of the evolution of the system.

We simulate our 5-site interaction CML Gauss map for  $\beta = 0.8$ ,  $\nu = 7.5$ , and  $N = 2 \times 10^5$ . The initial conditions are random and we average over  $1.2 \times 10^3$  configurations. We plot both  $P(t)$  and  $F(t)$  as a function of time  $t$  [see **Fig. 4 (a)** and **Fig. 5 (a)**]. From these plots, it can be seen that for  $\epsilon < \epsilon_c$ ,  $F(t)$  saturates and the  $P(t)$  decays exponentially as expected. Similarly, for  $\epsilon > \epsilon_c$ ,  $P(t)$  saturates and  $F(t)$  decays exponentially. At critical point  $\epsilon = \epsilon_c = 3.51475$ , we observe  $P(t) \sim t^{-\theta}$  and  $F(t) \sim t^{-\delta}$ . The persistence decays with the exponent  $\theta = 1.5$  while flip rate decays with exponent  $\delta = 0.159$ . If  $P(t) \sim t^{-\theta}$  and  $F(t) \sim t^{-\delta}$  then  $P(t)t^\theta$  and  $F(t)t^\delta$  should be constant asymptotically. We plot  $P(t)t^\theta$  and  $F(t)t^\delta$  as a function of  $t$  for  $\epsilon < \epsilon_c$ ,  $\epsilon > \epsilon_c$  and at  $\epsilon = \epsilon_c$  [see **Fig. 4 (b)** and **Fig. 5 (b)**]. We find that both the quantity tends to a constant for  $\epsilon = \epsilon_c$  as  $t \rightarrow \infty$ . For  $\epsilon \neq \epsilon_c$ , the curve displays upward or downward curvature. This is alternative evidence for the confirmation of the obtained values of the exponent. The exponent  $\delta$  and  $\theta$  match with DP exactly.

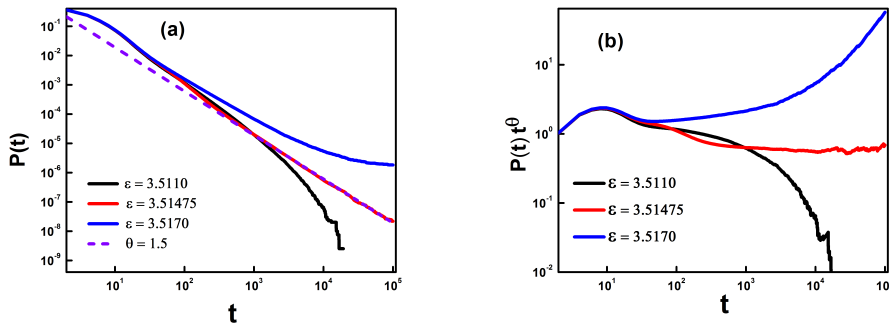


Fig. 4: **(a)** Plot of persistence  $P(t)$  as a function of time  $t$  for  $\epsilon < \epsilon_c$ ,  $\epsilon > \epsilon_c$  and at  $\epsilon = \epsilon_c$  for  $N = 2 \times 10^5$ . We average over a  $1.2 \times 10^3$  configuration. We observe that  $P(t) \sim t^{-\theta}$ ,  $\theta = 1.5$  at  $\epsilon = \epsilon_c = 3.51475$ . **(b)** Plot of  $P(t)t^\theta$  as a function of  $t$ , for  $\epsilon < \epsilon_c$ ,  $\epsilon > \epsilon_c$  and at  $\epsilon = \epsilon_c$  for the same data as **(a)**.

To confirm the nature of transition, we carry finite-size and off-critical scaling to compute the exponents  $z$  and  $\nu_{||}$ . This exercise is carried out for both order parameter  $F(t)$  as well as persistence  $P(t)$ . To compute dynamic exponent  $z$ , we carry out finite-size scaling simulations for distinct lattice sizes at  $\epsilon = \epsilon_c$ . To compute  $\nu_{||}$ , we carry out off-critical scaling. For this, we simulate a very large size lattice for various values of  $\epsilon$  both above and below  $\epsilon_c$ . We consider a lattice of size  $N = 10^5$  large enough so that finite size corrections are not important.

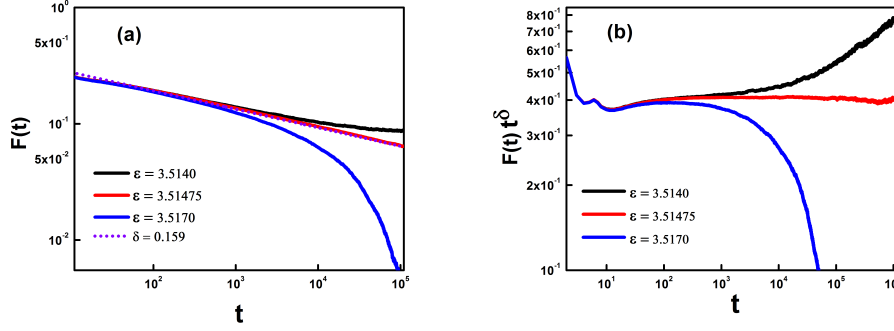


Fig. 5: **(a)** Plot of Flip rate  $F(t)$  as a function of time  $t$  for  $\epsilon < \epsilon_c$ ,  $\epsilon > \epsilon_c$  and at  $\epsilon = \epsilon_c$  for  $N = 2 \times 10^5$ . We average over a  $1.2 \times 10^3$  configuration. We observe  $F(t) \sim t^{-\delta}$ ,  $\delta = 0.159$  at  $\epsilon = \epsilon_c = 3.51475$ . **(b)** Plot of  $F(t)t^\delta$  as a function of time  $t$ , for  $\epsilon < \epsilon_c$ ,  $\epsilon > \epsilon_c$  and at  $\epsilon = \epsilon_c$  for the same data as **(a)**.

The scaling law for  $P(t)$  and  $F(t)$  hold to expect following relations:

$$P_N(t) = t^{-\theta} G(t/N^z, t\Delta^{\nu_{\parallel}}) \quad (8)$$

$$F_N(t) = t^{-\delta} G(t/N^z, t\Delta^{\nu_{\parallel}}) \quad (9)$$

where  $F$  and  $G$  are scaling function and  $\Delta = |\epsilon - \epsilon_c|$  departure from critical point. Thus for  $\Delta = 0$ , *i.e.*  $\epsilon = \epsilon_c$ , we obtain

$$P_N(t) = t^{-\theta} G(t/N^z) \quad (10)$$

$$F_N(t) = t^{-\delta} G(t/N^z) \quad (11)$$

and as  $N \rightarrow \infty$ , we obtain

$$P_N(t) = t^{-\theta} G(t\Delta^{\nu_{\parallel}}) \quad (12)$$

$$F_N(t) = t^{-\delta} G(t\Delta^{\nu_{\parallel}}) \quad (13)$$

We simulate the lattice for  $N = 50, 100, 200, 400, 800$ , and  $1600$  and average over more than  $1.2 \times 10^4$  configurations. We plot  $P(t)N^{\theta z}$  as a function of  $t/N^z$  at critical point  $\epsilon = \epsilon_c = 3.51475$  and the good scaling collapse is obtained at  $z = 1.58$  which is shown in **Fig. 6 (a)**. Similarly, we also plot  $F(t)N^{\delta z}$  as a function of  $t/N^z$  and the fine collapse is obtained at  $z = 1.58$  [see **Fig. 6 (b)**]. The obtained values of dynamic exponent for both  $P(t)$  and  $F(t)$  exactly match the dynamic exponent  $z = 1.58$  of the DP class.

We note that for  $\epsilon < \epsilon_c$ ,  $P(t)$  decays to zero exponentially and  $F(t)$  saturates. For  $\epsilon > \epsilon_c$ ,  $F(t)$  decays to zero and  $P(t)$  saturates. We simulate a large lattice of size  $10^5$  and average over more than  $800$  configurations for several values of  $\epsilon$  above and below  $\epsilon_c$ . We plot  $P(t)\Delta^{-\theta\nu_{\parallel}}$  as a function of  $t\Delta^{\nu_{\parallel}}$  and the good scaling collapse is obtained for  $\nu_{\parallel} = 1.73$ . This behavior is shown in **Fig. 7 (a)**. Similarly, we plot  $F(t)\Delta^{-\delta\nu_{\parallel}}$  as a function of  $t\Delta^{\nu_{\parallel}}$  and a good scaling collapse is obtained at  $\nu_{\parallel} = 1.73$ . This collapse is shown in **Fig. 7 (b)**. The obtained values of  $\nu_{\parallel} = 1.73$  match with the exponent of the DP class exactly.

We expect the flip rate  $F(t)$  scale as  $F(\infty) \propto \Delta^\beta$ , where  $\Delta = |\epsilon - \epsilon_c|$  and  $\beta = \nu_{\parallel} \delta$ . Similarly, the persistence  $P(\infty) \propto \Delta^{\beta'}$ , where  $\Delta = |\epsilon - \epsilon_c|$  and  $\beta' = \nu_{\parallel} \theta$ . We consider

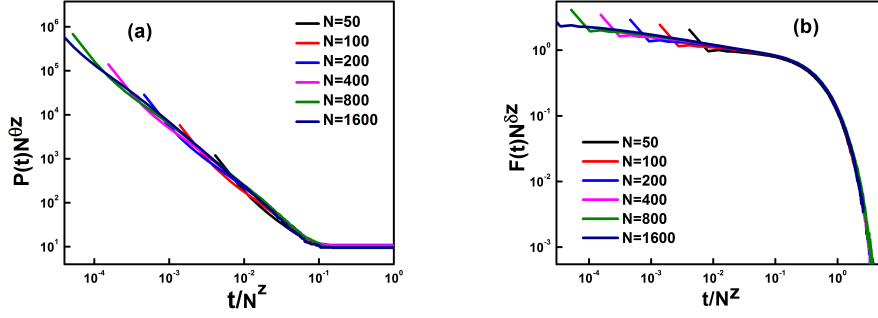


Fig. 6: (a) Plot of  $P(t)N^{\theta z}$  as a function of  $t/N^z$  at  $\epsilon = \epsilon_c = 3.51475$ . A good scaling collapse is observed at  $z = 1.58$  and  $\delta = 0.159$ . (b) Plot of  $F(t)N^{\delta z}$  as a function of  $t/N^z$  at  $\epsilon = \epsilon_c = 3.51475$ . The fine collapse is observed at  $z = 1.58$  and  $\theta = 1.5$ .

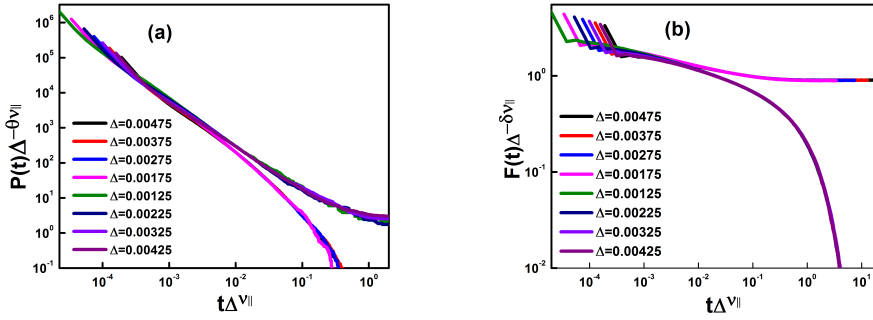


Fig. 7: We simulate a lattice of size  $N = 1 \times 10^5$  and each average over more than 800 configurations for several values of  $\epsilon$  above and below  $\epsilon_c$ . (a) We plot  $P(t)\Delta^{-\theta\nu_{||}}$  as a function of  $t\Delta^{\nu_{||}}$  for  $\epsilon < \epsilon_c$  and for  $\epsilon > \epsilon_c$ . The good scaling collapse is observed at  $\nu_{||} = 1.73$ . (b) We plot  $F(t)\Delta^{-\delta\nu_{||}}$  as a function of  $t\Delta^{\nu_{||}}$ . The good scaling collapse is observed at  $\nu_{||} = 1.73$ .

$N = 2 \times 10^5$  and average over a 50 configurations for both  $F(t)$  and  $P(t)$ . We plot  $\Delta = |\epsilon - \epsilon_c|$  versus  $P(\infty)$  in **Fig. 8 (a)**. The exponent  $\beta' = 2.595$ . Similarly, we plot  $\Delta = |\epsilon - \epsilon_c|$  versus  $F(\infty)$  in **Fig. 8 (b)**. The exponent  $\beta$  is found to be 0.276. These exponents are close to the expected value. They confirm the expected value of  $\nu_{||}$

### 3.2 Coupled map lattice with 3-site interaction

We also explore coupled Gauss maps with three-site interactions. We choose the map parameters of the Gauss map  $\nu = 7.5$ ,  $\beta = 0.6$ , and plot the bifurcation diagram. We consider a lattice size of  $N = 500$  and wait for  $t = 10^5$  time steps. The resulting bifurcation plot displays all values of sites as a function of coupling strength  $\epsilon$ . We plot the bifurcation diagram in **Fig. 9**. We observe the series of transitions from a fully synchronized state to a chaotic state by varying a coupling parameter. For larger values of  $\epsilon$ , the system again displays a fully synchronized state.

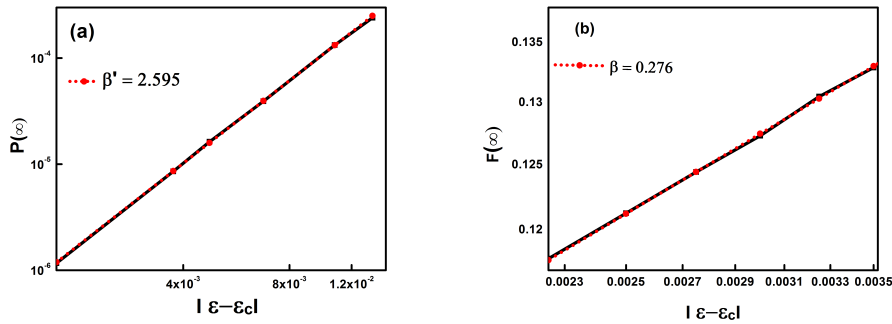


Fig. 8: We simulate a lattice of size  $N = 1 \times 10^5$  and each average 200 configurations for several values of  $\epsilon$  above and below  $\epsilon_c$ . (a) We plot  $\Delta = |\epsilon - \epsilon_c|$  versus  $P(\infty)$ . We find  $\beta' = 2.595$ . (b) We plot  $\Delta = |\epsilon - \epsilon_c|$  versus  $F(\infty)$ . We find  $\beta = 0.276$ .

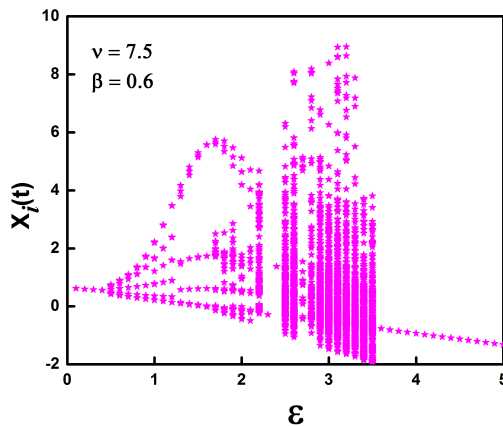


Fig. 9: Bifurcation diagram for 3-site interaction coupled Gauss maps where  $x_i(t)$  is plotted as a function of  $\epsilon$ . We fix  $\nu = 7.5$  and  $\beta = 0.6$  and simulate for  $N = 500$  and wait for  $t = 10^5$  time steps.

To study the nature of phase transition for  $\beta = 0.6$  and  $\nu = 7.5$ , we simulate the quantifiers  $F(t)$  and  $P(t)$  for distinct values of the coupling parameter  $\epsilon$ . We consider  $N = 2 \times 10^5$  and average over 400 configurations. We plot  $P(t)$  as a function of time steps  $t$  in **Fig. 10 (a)** and  $F(t)$  as a function of time steps  $t$  in **Fig. 11 (a)**. From this plot, we find that,  $F(t) \sim t^{-\delta}$  with  $\delta = 0.159$  and  $P(t) \sim t^{-\theta}$  with  $\theta = 1.5$  at critical point  $\epsilon = \epsilon_c = 3.57438$ . The obtained exponents exactly match with exponents of the DP class. We have shown  $P(t)t^\theta$  versus  $t$  and  $F(t)t^\delta$  versus  $t$  for  $\epsilon < \epsilon_c$ ,  $\epsilon > \epsilon_c$  and at  $\epsilon = \epsilon_c$  in **Fig. 10 (b)** and **Fig. 11 (b)**. We observe that the quantity  $F(t)$  and  $P(t)$  tends to a constant for  $\epsilon = \epsilon_c$  as  $t \rightarrow \infty$ . For  $\epsilon \neq \epsilon_c$ , the curve displays upward or downward curvature. This is alternative evidence for the confirmation of the obtained values of the exponent. The exponent  $\delta$  and  $\theta$  match with DP exactly. The multi-site interactions can also be termed as simplicial couplings.

Further, we study the finite-size scaling to compute the dynamic exponent  $z$ . We consider  $N = 50, 100, 200, 400, 800$  lattice sizes and average over more than  $4 \times 10^4$

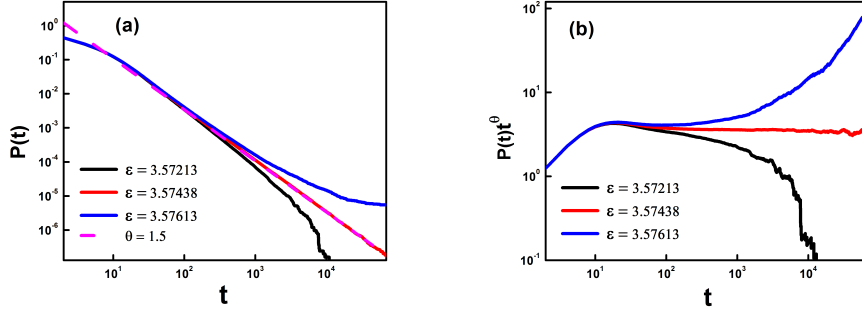


Fig. 10: **(a)** Plot of persistence  $P(t)$  as a function of time  $t$  for  $\epsilon < \epsilon_c$ ,  $\epsilon > \epsilon_c$  and at  $\epsilon = \epsilon_c$  for  $N = 2 \times 10^5$ . We average over a 400 configuration. We observe that  $P(t) \sim t^{-\theta}$ ,  $\theta = 1.5$  at  $\epsilon = \epsilon_c = 3.57438$ . **(b)** Plot of  $P(t)t^\theta$  as a function of  $t$ , for  $\epsilon < \epsilon_c$ ,  $\epsilon > \epsilon_c$  and at  $\epsilon = \epsilon_c = 3.57438$  for the same data as **(a)**.

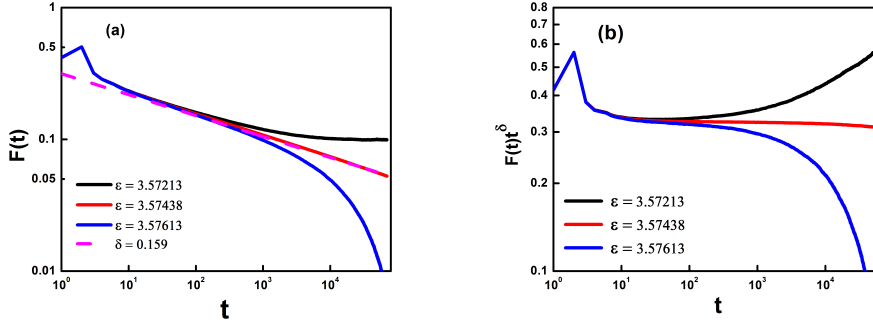


Fig. 11: **(a)** Plot of Flip rate  $F(t)$  as a function of time  $t$  for  $\epsilon < \epsilon_c$ ,  $\epsilon > \epsilon_c$  and at  $\epsilon = \epsilon_c$  for  $N = 2 \times 10^5$ . We average over a 400 configuration. We observe  $F(t) \sim t^{-\delta}$ ,  $\delta = 0.159$  at  $\epsilon = \epsilon_c = 3.57438$ . **(b)** Plot of  $F(t)t^\delta$  as a function of time  $t$ , for  $\epsilon < \epsilon_c$ ,  $\epsilon > \epsilon_c$  and at  $\epsilon = \epsilon_c = 3.57438$  for the same data as **(a)**

configurations for both  $P(t)$  and  $F(t)$ . We plot  $P(t)N^{\theta z}$  versus  $t/N^z$  in **Fig. 12 (a)** and  $F(t)N^{\delta z}$  as a function of  $t/N^z$  in **Fig. 12 (b)** at  $\epsilon = \epsilon_c = 3.57438$ . From this plot, we observe that for  $P(t)$  a good scaling collapse is observed for  $z = 1.58$  and  $\theta = 1.5$ . While for  $F(t)$  a good scaling collapse is observed for  $z = 1.58$  and  $\delta = 0.159$ . The exponent obtained from finite size scaling for both  $P(t)$  and  $F(t)$  is exactly the same as the exponent of the DP universality class.

We study off-critical scaling to compute the exponent  $\nu_{\parallel}$ . We simulate the lattice for distinct values of  $\epsilon$  for above and below the critical point. We consider  $N = 2 \times 10^5$  and average over a 100 configuration. We plot  $P(t)\Delta^{-\theta\nu_{\parallel}}$  as a function of  $t\Delta^{\nu_{\parallel}}$  and the good scaling collapse is obtained for  $\nu_{\parallel} = 1.73$ . This behavior is shown in **Fig. 13 (a)**. Similarly, we plot  $F(t)\Delta^{-\delta\nu_{\parallel}}$  as a function of  $t\Delta^{\nu_{\parallel}}$  and a good scaling collapse is obtained at  $\nu_{\parallel} = 1.73$ . This collapse is shown in **Fig. 13 (b)**. The obtained values of  $\nu_{\parallel} = 1.73$  match with the exponent of the DP class exactly.

We expect the flip rate  $F(t)$  scale as  $F(\infty) \propto \Delta^\beta$ , where  $\Delta = |\epsilon - \epsilon_c|$  and  $\beta = \nu_{\parallel} \delta$ . Similarly, the persistence  $P(\infty) \propto \Delta^{\beta'}$ , where  $\Delta = |\epsilon - \epsilon_c|$  and  $\beta' = \nu_{\parallel} \theta$ . We

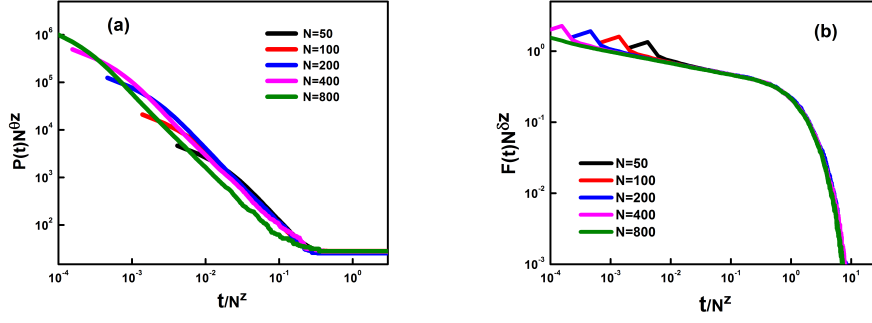


Fig. 12: **(a)** Plot of  $P(t)N^{\theta z}$  as a function of  $t/N^z$  at  $\epsilon = \epsilon_c = 3.57438$  and  $\theta=1.5$ . A good scaling collapse is observed at  $z = 1.58$  and  $\theta = 1.5$ . **(b)** Plot of  $F(t)N^{\delta z}$  as a function of  $t/N^z$  at  $\epsilon = \epsilon_c = 3.57438$ . The fine collapse is observed at  $z = 1.58$  and  $\delta=0.159$ .

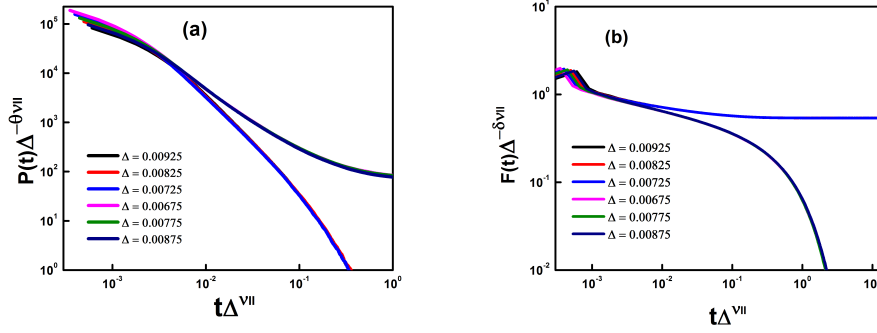


Fig. 13: We simulate a lattice of size  $N = 2 \times 10^5$  and each average over more than 100 configurations for several values of  $\epsilon$  above and below  $\epsilon_c$ . **(a)** We plot  $P(t)\Delta^{-\theta\nu_{||}}$  as a function of  $t\Delta^{\nu_{||}}$  for  $\epsilon < \epsilon_c$  and for  $\epsilon > \epsilon_c$ . The good scaling collapse is observed at  $\nu_{||} = 1.73$ . **(b)** We plot  $F(t)\Delta^{-\delta\nu_{||}}$  as a function of  $t\Delta^{\nu_{||}}$ . The good scaling collapse is observed at  $\nu_{||} = 1.73$ .

consider  $N = 2 \times 10^5$  and average over a 50 configurations for both  $F(t)$  and  $P(t)$ . We plot  $P(\infty)$  versus  $\Delta=|\epsilon - \epsilon_c|$  in **Fig. 14 (a)** and the exponent  $\beta'$  is found to be 2.595. Similarly, we plot  $F(\infty)$  versus  $\Delta=|\epsilon - \epsilon_c|$  in **Fig. 14 (b)** and the exponent  $\beta$  is found to be 0.276. This is further confirmation of the exponent  $\nu_{||}$

### 3.3 Coupled map lattice with 4-site interaction

We also investigate the nature of the phase transition for even site interaction in a coupled Gauss map. We simulate our model for 4-site interaction. We choose the map parameters  $\beta = 0.8$  and  $\nu = 7.5$  and plot the bifurcation diagram for  $N = 500$  after waiting for  $t = 10^5$  steps. We plot the bifurcation diagram in **Fig. 15**. The bifurcation diagram is useful for visualization of the behavior of the system as a function of the coupling parameter. The bifurcation diagram captures the transition from a fully synchronized state to chaos. As the coupling parameter is increased

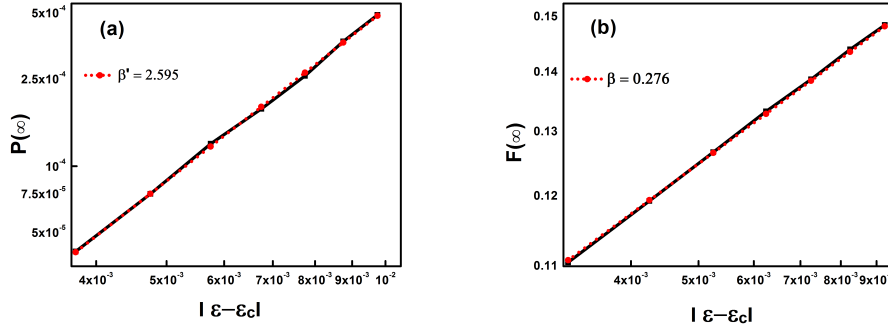


Fig. 14: We simulate a lattice of size  $N = 1 \times 10^5$  and each average 200 configurations for several values of  $\epsilon$  above and below  $\epsilon_c$ . (a) We plot  $P(\infty)$  versus  $\Delta = |\epsilon - \epsilon_c|$ . We find  $\beta' = 2.595$ . (b) We plot  $F(\infty)$  versus  $\Delta = |\epsilon - \epsilon_c|$ . We find  $\beta = 0.276$ .

further, the system reaches a synchronized state. We focus on one of the transitions to synchronization that shows continuous transition.

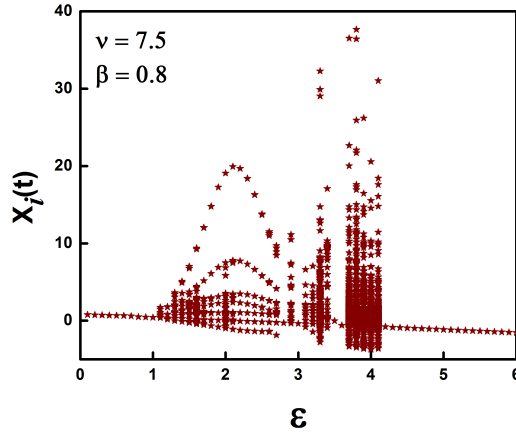


Fig. 15: Bifurcation diagram for 4-site interaction coupled Gauss maps where  $x_i(t)$  is plotted as a function of  $\epsilon$ . We fix  $\nu = 7.5$  and  $\beta = 0.8$  and simulate for  $N = 500$  and wait for  $t = 10^5$  time steps.

We compute the flip rate  $F(t)$  and persistence  $P(t)$  as the order parameter at the transition point for this system. We consider  $N = 2 \times 10^5$  and average over a 200 configuration. We plot  $F(t)$  as a function of time steps  $t$  in **Fig. 16 (a)**. We observe that  $F(t)$  shows power-law decay with logarithmic oscillation at  $\epsilon = \epsilon_c = 4.19611758$ . The decay exponent is found to be  $\delta = 0.354$ . We have displayed the  $F(t)t^\delta$  as a function of  $t$  for the same data in the inset plot. This plot confirms a clear oscillation over and above the power-law. Similarly, we plot  $P(t)$  as a function of time  $t$  in **Fig. 16 (b)**. We find that  $P(t)$  shows power-law decay superposed with logarithmic oscillations at  $\epsilon = \epsilon_c = 4.19611758$ . The decay exponent is found to be  $\theta = 1$ . We also plot  $F(t)t^\theta$  as a function of  $t$  for the same data in the inset plot. This plot displays

oscillations over and above the power-law that confirm the  $\theta$  values and logarithmic oscillation. This provides a novel transition with an exponent that does not match DP for both persistence exponent  $\delta$  or  $\theta$ . Therefore, the 4-site interaction is a relevant perturbation that emerges in a novel transition for the Gauss map.

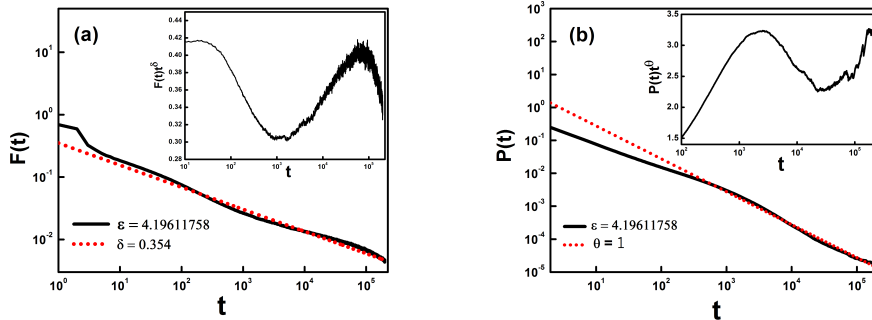


Fig. 16: Plot of 4-site interaction coupled Gauss map for  $N = 2 \times 10^5$  and average over 200 configurations. **(a)** Main Figure: Plot of  $F(t)$  as a function of  $t$  at  $\epsilon = \epsilon_c = 4.19611758$ .  $F(t)$  show the clear logarithmic oscillation with  $\delta = 0.354$ . Inset: Plot of  $F(t)t^\delta$  as a function of  $t$ . **(b)** Main Figure: Plot of  $P(t)$  as a function of  $t$ , at  $\epsilon = \epsilon_c = 4.19611758$ .  $P(t)$  show the clear logarithmic oscillation with  $\theta = 1$ . Inset: Plot of  $P(t)t^\theta$  as a function of  $t$ .

### 3.4 Coupled map lattice with 2-site interaction

Lastly, we investigate the model with 2-site interaction. We consider  $N = 500$ , wait for  $t = 10^5$ , and plot the bifurcation diagram for  $\beta = 0.9$  and  $\nu = 7.8$ . The bifurcation diagram depicts the behavior of the system as a function of the coupling strength. **Fig. 17** shows the bifurcation diagram. From this plot, we find that the system displays a fully synchronized state for low coupling. A transition occurs at  $\epsilon = 1.5$  and again for  $2.1 \leq \epsilon \leq 2.4$ , and the system transitions to a synchronized state. We again investigate the point that shows a continuous transition.

We compute the flip rate  $F(t)$  and persistence  $P(t)$  for  $N = 4 \times 10^4$  and average over a 1200 configuration. **Fig. 18 (a)** shows the plot  $F(t)$  as a function of time  $t$ . The inset on the main figure shows the plot of  $F(t)t^\delta$  as a function of  $t$ . We find  $F(t) \sim t^{-\delta}$  at  $\epsilon = \epsilon_c = 2.338$ . The decay exponent is found to be  $\delta = 1.12$ . This exponent is very different from the DP class. We also plot  $P(t)$  as a function of  $\log(t)$  in **Fig. 18 (b)**. It decays as  $\log(t)^{-\theta'}$ . The inset shows a plot of  $P(t)\log(t)^{\theta'}$  as a function of  $t$  with  $\theta' = 0.154$ . The persistence decays slower than power-law in this case and there is no well-defined persistence exponent.

## Summary

Directed percolation is one of the most widely observed non-equilibrium dynamic transitions to an absorbing state. Of late, it has been observed in experimental situations as well. Most of these systems are modeled by equations involving a Laplacian.

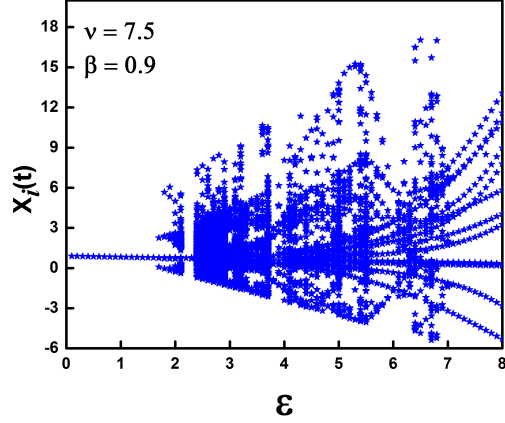


Fig. 17: Plot of bifurcation diagram for 2-site interaction coupled Gauss maps where  $x_i(t)$  is plotted as a function of  $\epsilon$ . We fix  $\nu = 7.5$ ,  $\beta = 0.9$  and simulate for  $N = 500$  and  $t = 10^5$  time steps.

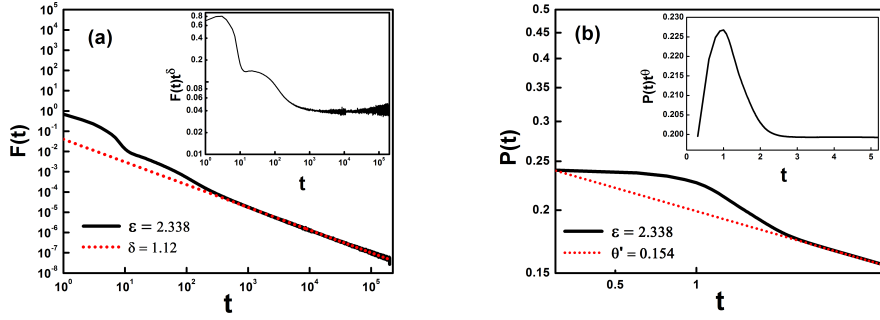


Fig. 18: Plot of 2-site interaction coupled Gauss map for  $N = 4 \times 10^4$  and average over a 1200 configuration. **(a)** Main Figure: Plot of  $F(t)$  as a function of  $t$  for  $\epsilon = \epsilon_c = 2.338$ . We carry out a running time average to reduce fluctuations. We find  $F(t) \sim t^{-\delta}$  with  $\delta = 1.12$ . Inset:  $F(t)t^\delta$  as a function of  $t$ . **(b)** Main Figure: Plot of  $P(t)$  as a function of  $\log(t)$  for  $\epsilon = \epsilon_c = 2.338$ . We find  $P(t) \sim 1/\log(t)^{\theta'}$  with  $\theta' = 0.154$ . Inset: Plot of  $P(t)\log(t)^{\theta'}$  as a function of  $t$ .

The standard formulation of coupled map lattices can be considered as discretized Laplacian. It involves pairwise interactions. This model is not a discretized Laplacian and the interactions are multi-body multiplicative interactions.

In this work, we study the coupled Gauss map for odd and even site interaction in one dimension. We study 3-site and 5-site for odd sites and 2-site and 4-site for even sites interaction. The coupling is such that it cannot be decomposed into pairwise interactions. We have classified the sites, considering fixed points as a reference. If the variable values are above or below the fixed point, then the associate spin is (+1) or (-1). We investigate the phase transition using quantifiers such as the flip rate  $F(t)$  and persistence  $P(t)$ .

*i)* For 3-site and 5-site interaction, we find the power-law decay of flip rate  $F(t)$  and persistence  $P(t)$  at a critical point. The decay exponent for  $F(t)$  is  $\delta=0.159$  and for  $P(t)$  is  $\theta=1.5$ . We also study the finite-size scaling and the off-critical scaling. The obtained exponents  $z = 1.5$ ,  $\nu_{\parallel} = 1.73$ , and  $\beta=0.275$  match exactly with the exponents of the DP universality class. Thus DP class is robust for 3-site and 5-site interaction studied in this work.

*ii)* For even site interaction, the exponents change. For 4-site interaction, we find the decay exponent  $\delta = 0.354$  and  $\theta = 1$ . We observe the logarithmic oscillations over and above the power-law. For 2-site interaction, we find the decay exponent  $\delta=1.12$ . The persistence decays slower than power-law as  $\log(t)^{-\theta'}$ . The behaviors are different from DP and they are different from each other. Thus, multi-site couplings could lead to a new universality class. It could depend on the number of coupled sites. It could also depend on the detailed nature of the map. Further studies on different maps as well as interactions could be of interest. The results are quite surprising given the fact that only a few universality classes are known for absorbing state transitions.

## Acknowledgments

PMG thanks DST-SERB (CRG/2020/003993) for financial assistance.

## Author Contribution

MCW and PMG contributed to conceptualization, simulations, visualization, and drafting.

## Statements and Declarations

The authors declare that they have no conflict of interest.

## Data Availability Statement:

This manuscript has no associated data or the data will not be deposited. [Author's comment: All data that support the plots within the paper and other findings of the study are available from the first author upon reasonable request.]

## References

1. AV Andreev, NS Frolov, AN Pisarchik, and AE Hramov. Chimera state in complex networks of bistable hodgkin-huxley neurons. *Phys. Rev. E*, 100(2):022224, 2019.
2. Luciano da Fontoura Costa, Osvaldo N Oliveira Jr, Gonzalo Travieso, Francisco Aparecido Rodrigues, Paulino Ribeiro Villas Boas, Lucas Antiqueira, Matheus Palhares Viana, and Luis Enrique Correa Rocha. Analyzing and modeling real-world phenomena with complex networks: a survey of applications. *Adv. Phys.*, 60(3):329–412, 2011.
3. Oliver M Cliff, Vitali Sintchenko, Tania C Sorrell, Kiranmayi Vadlamudi, Natalia McLean, and Mikhail Prokopenko. Network properties of salmonella epidemics. *Sci. Rep.*, 9(1):1–6, 2019.
4. Upinder S Bhalla and Ravi Iyengar. Emergent properties of networks of biological signaling pathways. *Science*, 283(5400):381–387, 1999.

5. Rushed Kanawati. Multiplex network mining: A brief survey. *IEEE Intell. Informatics Bull.*, 16(1):24–27, 2015.
6. Arindam Mishra, Suman Saha, M Vigneshwaran, Pinaki Pal, Tomasz Kapitaniak, and Syamal K Dana. Dragon-king-like extreme events in coupled bursting neurons. *Phys. Rev. E*, 97(6):062311, 2018.
7. Ernesto Estrada and Juan A Rodríguez-Velázquez. Subgraph centrality and clustering in complex hyper-networks. *Phys. A: Stat. Mech. Appl.*, 364:581–594, 2006.
8. Philip S Chodrow. Configuration models of random hypergraphs. *J Complex Netw*, 8(3):cnaa018, 2020.
9. G. Karypis, R. Aggarwal, V. Kumar, and S. Shekhar. Multilevel hypergraph partitioning: applications in vlsi domain. *IEEE Trans. Very Large Scale Integr. VLSI Syst.*, 7(1):69–79, 1999.
10. Giovanni Petri, Paul Expert, Federico Turkheimer, Robin Carhart-Harris, David Nutt, Peter J Hellyer, and Francesco Vaccarino. Homological scaffolds of brain functional networks. *J. R. Soc. Interface*, 11(101):20140873, 2014.
11. Ana P Millán, Joaquín J Torres, and Ginestra Bianconi. Explosive higher-order kuramoto dynamics on simplicial complexes. *Phys. Rev. Lett.*, 124(21):218301, 2020.
12. Per Sebastian Skardal and Alex Arenas. Higher order interactions in complex networks of phase oscillators promote abrupt synchronization switching. *Commun. Phys.*, 3(1):1–6, 2020.
13. Lucia Valentina Gambuzza, Francesca Di Patti, Luca Gallo, Stefano Lepri, Miguel Romance, Regino Criado, Mattia Frasca, Vito Latora, and Stefano Boccaletti. Stability of synchronization in simplicial complexes. *Nat. Commun.*, 12(1):1255, 2021.
14. Sudepto Bhattacharya. Higher-order social-ecological network as a simplicial complex. *arXiv preprint arXiv:2112.15318*, 2021.
15. Vsevolod Salnikov, Daniele Cassese, and Renaud Lambiotte. Simplicial complexes and complex systems. *Eur. J. Phys.*, 40(1):014001, 2018.
16. Reza Ghorbanchian, Juan G Restrepo, Joaquín J Torres, and Ginestra Bianconi. Higher-order simplicial synchronization of coupled topological signals. *Commun. Phys.*, 4(1):120, 2021.
17. Malayaja Chutani, Bosiljka Tadić, and Neelima Gupte. Hysteresis and synchronization processes of kuramoto oscillators on high-dimensional simplicial complexes with competing simplex-encoded couplings. *Phys. Rev. E*, 104(3):034206, 2021.
18. Ajay Deep Kachhvah and Sarika Jalan. First-order route to antiphase clustering in adaptive simplicial complexes. *Phys. Rev. E*, 105(6):L062203, 2022.
19. Joan T Matamalas, Sergio Gómez, and Alex Arenas. Abrupt phase transition of epidemic spreading in simplicial complexes. *Phys. Rev. Res.*, 2(1):012049, 2020.
20. Sarika Jalan and Ayushi Suman. Multiple first-order transitions in simplicial complexes on multilayer systems. *Phys. Rev. E*, 106(4):044304, 2022.
21. Priyanka D. Bhojar, Naval R. Sabe, and Prashant M. Gade. Dynamical phases and phase transition in simplicially coupled logistic maps. *Int. J. Mod. Phys. C.*, in press, 2025.
22. Mahtab Mehrabbeik, Sajad Jafari, and Matjaž Perc. Synchronization in simplicial complexes of memristive rulkov neurons. *Front. Comput. Neurosci.*, 17:1248976, 2023.
23. Raissa M D’Souza, Jesus Gómez-Gardenes, Jan Nagler, and Alex Arenas. Explosive phenomena in complex networks. *Adv. Phys.*, 68(3):123–223, 2019.
24. Vinod Patidar. Co-existence of regular and chaotic motions in the gaussian map. *Electron. J. Theor. Phys.*, 3(13), 2006.
25. Satya N Majumdar. Persistence in nonequilibrium systems. *Curr. Sci.*, pages 370–375, 1999.
26. Nitesh D Shambharkar and Prashant M Gade. Universality of the local persistence exponent for models in the directed ising class in one dimension. *Phys. Rev. E*, 100(3):032119, 2019.
27. Haye Hinrichsen and Hari M Koduvely. Numerical study of local and global persistence in directed percolation. *Eur. Phys. J. B*, 5(2):257–264, 1998.

28. Ezequiel V Albano and Miguel A Munoz. Numerical study of persistence in models with absorbing states. *Phys. Rev. E*, 63(3):031104, 2001.
29. Johannes Fuchs, Jörg Schelter, Francesco Ginelli, and Heye Hinrichsen. Local persistence in the directed percolation universality class. *J. Stat. Mech.: Theory Exp.*, 2008(04):P04015, 2008.
30. Gautam I Menon, Sudeshna Sinha, and Purusattam Ray. Persistence at the onset of spatio-temporal intermittency in coupled map lattices. *EPL*, 61(1):27, 2003.
31. Zahera Jabeen and Neelima Gupte. Dynamic characterizers of spatiotemporal intermittency. *Phys. Rev. E*, 72(1):016202, 2005.
32. Volker Ahlers and Arkady Pikovsky. Critical properties of the synchronization transition in space-time chaos. *Phys. Rev. Lett.*, 88(25):254101, 2002.
33. Sumit S Pakhare and Prashant M Gade. Novel transition to fully absorbing state without long-range spatial order in directed percolation class. *Commun Nonlinear Sci Numer Simul*, 85:105247, 2020.
34. Pratik M Gaiki, Ankosh D Deshmukh, Sumit S Pakhare, and Prashant M Gade. Transition to period-3 synchronized state in coupled gauss maps. *Chaos*, 34(2):023113, 2024.
35. Divya D Joshi and Prashant M Gade. Cellular automata model for period-n synchronization: a new universality class. *J. Phys. A*, 58(2):02LT01, 2024.
36. Björn Hof. Directed percolation and the transition to turbulence. *Nat. Rev. Phys.*, 5(1):62–72, 2023.
37. Kazumasa A Takeuchi, Masafumi Kuroda, Hugues Chaté, and Masaki Sano. Experimental realization of directed percolation criticality in turbulent liquid crystals. *Phys. Rev. E Stat. Nonlin. Soft Matter Phys.*, 80(5):051116, 2009.
38. Hans-Karl Janssen. On the nonequilibrium phase transition in reaction-diffusion systems with an absorbing stationary state. *Z. Phys.*, 42(2):151–154, 1981.
39. P. Grassberger. On phase transitions in schlögl's second model. In Christian Vidal and Adolphe Pacault, editors, *Nonlinear Phenomena in Chemical Dynamics*, pages 262–262, Berlin, Heidelberg, 1981. Springer Berlin Heidelberg.
40. Priyanka D Bhojar, Manoj C Warambhe, Swapnil Belkhude, and Prashant M Gade. Robustness of directed percolation under relaxation of prerequisites: role of quenched disorder and memory. *Eur. Phys. J. B*, 95(4):1–11, 2022.
41. Hugues Chaté and Paul Manneville. Spatio-temporal intermittency in coupled map lattices. *Phys. D: Nonlinear Phenom.*, 32(3):409–422, 1988.
42. Alex Yu Tretyakov, Norio Inui, and Norio Konno. Phase transition for the one-sided contact process. *J. Phys. Soc. Jpn.*, 66(12):3764–3769, 1997.
43. TM Janaki, Sudeshna Sinha, and Neelima Gupte. Evidence for directed percolation universality at the onset of spatiotemporal intermittency in coupled circle maps. *Phys. Rev. E*, 67(5):056218, 2003.